J. Fluid Mech. (1996), *vol.* 314, *pp.* 113–138

First- and higher-order effects of curvature and torsion on the flow in a helical rectangular duct

By C. JONAS BOLINDER

Division of Fluid Mechanics, Lund Institute of Technology, Box 118, 221 00 Lund, Sweden

(Received 17 February 1995 and in revised form 29 December 1995)

A series expansion method is employed to determine the first-order terms in curvature ϵ and torsion η of fully developed laminar flow in helical square ducts and in helical rectangular ducts of aspect ratio two. The first-order solutions are compared to solutions of the full governing equations. For toroidal square ducts with zero pitch, the first-order solution is fairly accurate for Dean numbers, $De = Re\,\epsilon^{1/2}$, up to about 20, and for straight twisted square ducts the first-order solution is accurate for Germano numbers, $Gn = \eta\, Re$, up to at least 50 where Re is the Reynolds number. Important conclusions are that the flow in a helical duct with a finite pitch or torsion to the first order (i.e. with higher-order terms in ϵ and η neglected) is obtained as a superposition of the flow in a toroidal duct with zero pitch and a straight twisted duct; that the secondary flow in helical non-circular ducts for sufficiently small Re is dominated by torsion effects; and that for increasing Re, the secondary flow eventually is dominated by effects due to curvature. Torsion has a stronger impact on the flow for aspect ratios greater than one. A characteristic combined higher-order effect of curvature and torsion is an enlargement of the lower vortex of the secondary flow at the expense of the upper vortex, and also a shift of the maximum axial flow towards the upper wall. For higher Reynolds numbers, bifurcation phenomena appear. The extent of a few solution branches for helical ducts with finite pitch or torsion is determined. For ducts with small torsion it is found that the extent of the stable solution branches is affected little by torsion. Physical velocity components are employed to describe the flow. The contravariant components are found useful when describing the convective transport in the duct.

1. Introduction

Curved ducts appear in various industrial applications, and a detailed knowledge of the fluid flow behaviour is important to be able to predict for example the pressure drop and heat and mass transfer characteristics. The curvature induces a secondary flow in the duct, which often is found to give increased heat and mass transfer rates.

Previous work on curved duct flows is referred to in the review articles by Berger, Talbot & Yao (1983), Nandakumar & Masliyah (1986), Ito (1987) and Berger (1991). From these, it is evident that most theoretical studies concern toroidally curved ducts with zero pitch and with a circular cross-section. A toroidally curved duct with zero pitch is characterized by the centreline having a constant curvature κ, which is equal to the inverse of the radius of curvature. Helically coiled ducts with a finite pitch are often used in practice, and they are characterized by the centreline having a constant curvature and a constant torsion τ. A straight twisted duct is obtained in the limit when the curvature tends to zero and while the torsion remains finite. A non-zero torsion

implies that a non-orthogonal coordinate system is the most appropriate one in a theoretical analysis.

Flow in toroidally curved ducts with zero pitch has been the subject of numerous theoretical studies, ever since the pioneering work by Dean (1927, 1928*a*). His name is given to the Dean number, $De = Re\,\epsilon^{1/2}$, where the Reynolds number Re is based on mean axial flow and hydraulic diameter d_h, and where the dimensionless curvature $\epsilon = \kappa d_h$. The Dean number fully characterizes the flow in a loosely coiled duct (i.e. with small curvature). Different definitions of the Dean number have been used in the literature, see Berger *et al.* (1983) for a review. The definition used in this paper is helpful because it is directly related to the Reynolds number of the flow.

Next, a few previous investigations considering toroidally curved rectangular ducts with zero pitch will be mentioned. Employing a series expansion method similar to the one by Dean (1927, 1928*a*), Ito (1951) and Cuming (1952) independently determined the first-order contributions to the flow in toroidally curved ducts of elliptical and rectangular cross-sections. The rectangular cross-section is less amenable to an analytical treatment, since each individual term of the power series in ϵ is in turn obtained as an infinite series, and in general only a few terms of this series are determined. For example, the first-order secondary flow components obtained by Cuming (1952) for a square cross-section do not describe the two expected counter-rotating cells, so in this respect the analysis by Cuming is not sufficiently accurate. Mori, Uchida & Ukon (1971) performed a boundary layer analysis of the flow in a toroidal square duct with zero pitch. The boundary layer method is assumed to be valid for Dean numbers in the higher laminar regime; viscous effects are only considered in thin boundary layers close to the walls; in the central part of the duct, the fluid is assumed inviscid. A phenomenon that boundary layer theory fails to predict is the appearance of an extra vortex pair of the secondary flow near the outer wall of a curved square duct, when the Dean number is raised above a critical value of about 130. This phenomenon was first reported by Joseph, Smith & Adler (1975) and Cheng, Lin & Ou (1976), who independently solved the governing equations using a numerical method. The phenomenon is sometimes referred to as 'Dean's instability', after Dean (1928*b*), who analysed curved rectangular ducts of infinite aspect ratio, and found the primary flow to be unstable above a critical Dean number. The instability, which is of centrifugal nature, causes streamwise-orientated counter-rotating vortices, similar to the extra vortices in the square duct, see further e.g. Matsson & Alfredsson (1990). Winters (1987) performed an accurate determination of the solution structure for toroidal rectangular ducts with zero pitch. He discovered several solution branches, some of which were found to be unstable. The findings of Joseph *et al.* and Cheng *et al.* could now be explained as follows: the abrupt change of flow structure at the critical Dean number was due to a jump from the primary two-vortex S_1 branch to the four-vortex S_3 branch. Other references to the fully developed flow case are Ghia, Ghia & Shin (1987), Yanase & Nishiyama (1988), Daskopoulos & Lenhoff (1989), Thangam & Hur (1990) and Kao (1992). Duh & Shih (1989) examined inclined square cross-sections. Developing flow in toroidal rectangular ducts with zero pitch has been considered for example by Sankar, Nandakumar & Masliyah (1988), Soh (1988), Bara, Nandakumar & Masliyah (1992) and Mees (1994).

Among the first to analyse, from a theoretical point of view, the effect of a finite pitch or torsion on the flow were Murata *et al.* (1981), Wang (1981) and Germano (1982), who all considered ducts of circular cross-section. Wang and Germano both employed a series expansion method, but while Wang found a first-order effect of torsion on the secondary flow, Germano only found a second-order effect. The reason for the

discrepancy was that different velocity components were used for the secondary flow. Wang employed so-called contravariant components, and Germano employed physical components, i.e. the velocity vector was expanded in a physical (i.e. an orthonormal) basis. The contravariant components are obtained when the velocity is expanded in the natural basis of the coordinate system (see §2 for a definition). However, for a non-zero torsion, the natural basis is non-orthogonal, and it also varies over the cross-section of the duct. This makes the natural basis and the resulting contravariant components inconvenient to use. The preferred way to describe the flow is using physical velocity components obtained from a basis which is constant over the cross-section. Then, in particular, the components are obtained as projections of the velocity vector on the respective base vectors, and it is easy to realize the behaviour of the flow. Actually, the result by Germano (1982), that torsion has no first-order effect on the secondary flow for a circular duct, may also be deduced from pure geometrical considerations, as explained in the next section. For ducts of non-circular cross-section, however, torsion has a first-order effect on the secondary flow, as remarked by Germano (1989), who studied elliptical ducts. Murata *et al.* (1981) employed physical velocity components, as did Kao (1987), who investigated higher-Re laminar flow in helical circular ducts using a finite-difference method. Other authors on helical circular ducts with finite pitch are Tuttle (1990), Xie (1990), Chen & Jan (1992) and Liu & Masliyah (1993). Tuttle suggested that the discrepancy between the results of Wang (1981) and Germano (1982) could be explained by the circumstance that different frames of reference of the observer were employed. However, as discussed in Bolinder (1995*b*), this is not correct, since, in particular, the angular velocity ω which, according to Tuttle, should relate the two observers is not a constant, but varies over the cross-section of the duct. As remarked by Bolinder (1993) and Liu & Masliyah (1994), Xie (1990) fails to define a proper stream function for the secondary flow, and as a result of this, Xie predicts a turning of the secondary flow vortices due to the effect of torsion.

The effect of torsion on the flow in helical square ducts has been investigated by Bolinder (1993, 1995*a*, *b*), Chen & Jan (1993) and Bolinder & Sundén (1995). Bolinder (1993, 1995*b*) solved the governing equations using a finite-volume method. The two unconditionally stable solution branches (S_1 and S_5) detected for a toroidal square duct, were found to persist fairly unchanged if the duct was provided with a small torsion. This result contradicts the conclusion by Chen & Jan (1993) that 'Dean's instability' can be avoided due to the effect of torsion. Bolinder & Sundén (1995) give experimental confirmation of the numerical results for helical square ducts with finite pitch, and a few observations concerning transition to turbulence are also provided.

Flow in straight twisted ducts (with $\kappa = 0$) has been analysed by among others Germano (1989), who considered an elliptical cross-section. He pointed out that for a loosely twisted duct, i.e. with a small dimensionless torsion $\eta = \tau d_h$, the governing equations depend on a single similarity parameter $Gn = \eta Re$, which, following Liu & Masliyah (1993), we call the Germano number. For the same parameter, Germano (1989) used the notation T and Chen & Jan (1992) the notation Tn. Flow in straight twisted rectangular ducts has been studied by Masliyah & Nandakumar (1981), Nandakumar & Masliyah (1983) and Kheshgi (1993).

In the present study, the first-order terms in curvature ϵ and torsion η of the flow in a helical square duct and in a helical rectangular duct of aspect ratio two are explicitly determined by solving the appropriate first-order equations. The results are then compared to solutions obtained by solving the full unsimplified governing equations. In this way, the range of applicability of the first-order terms may be determined, and the character of the higher-order terms may be found in an indirect manner. Both the

first-order and the full governing equations are solved using a finite-volume method, which has proved effective in previous studies by the author.

2. Governing equations

The position vector of the centreline of a helical duct may be written

$$\boldsymbol{r}_c(s) = R\boldsymbol{e}_r(s) + K\vartheta(s)\,\boldsymbol{e}_z, \quad \text{where} \quad \vartheta(s) = s/(R^2+K^2)^{1/2}. \tag{1}$$

The parameter s, which is the arclength of the centreline, is used as a coordinate along the duct. ϑ is a polar angle, R is the radius of the cylinder round which the centreline is coiled, and $2\pi K$ is the so-called pitch, see figure 1; $\boldsymbol{e}_r$, $\boldsymbol{e}_\theta$ and $\boldsymbol{e}_z$ are unit base vectors of the cylindrical coordinate system indicated in figure 1. The tangent $\boldsymbol{t}$, normal $\boldsymbol{n}$ and binormal $\boldsymbol{b}$ of $\boldsymbol{r}_c$ are defined by

$$\boldsymbol{t} = \boldsymbol{r}_c', \quad \boldsymbol{n} = \frac{1}{\kappa}\boldsymbol{r}_c'', \quad \boldsymbol{b} = \boldsymbol{t}\times\boldsymbol{n}, \tag{2}$$

where a prime denotes a derivative with respect to s. Note that $\boldsymbol{t}$, $\boldsymbol{n}$ and $\boldsymbol{b}$ are orthonormal. For the helical centreline described by (1), one obtains

$$\left.\begin{aligned} \boldsymbol{t}(s) &= \cos\alpha\,\boldsymbol{e}_\theta(s) + \sin\alpha\,\boldsymbol{e}_z, \\ \boldsymbol{n}(s) &= -\boldsymbol{e}_r(s), \\ \boldsymbol{b}(s) &= -\sin\alpha\,\boldsymbol{e}_\theta(s) + \cos\alpha\,\boldsymbol{e}_z; \end{aligned}\right\} \tag{3}$$

α is the slope of the centreline relative to the plane z = constant. One finds that

$$\cos\alpha = \frac{R}{(R^2+K^2)^{1/2}}, \quad \sin\alpha = \frac{K}{(R^2+K^2)^{1/2}}. \tag{4}$$

The curvature κ and the torsion τ of $\boldsymbol{r}_c$ are defined by

$$\kappa = |\boldsymbol{r}_c''|, \quad \tau = \boldsymbol{n}'\cdot\boldsymbol{b}. \tag{5}$$

Equation (1) gives

$$\kappa = \frac{R}{R^2+K^2}, \quad \tau = \frac{K}{R^2+K^2}. \tag{6}$$

It is illustrative to evaluate (3), (4) and (6) for the special cases of a toroidal duct ($K = \tau = 0$) and a straight twisted duct ($R = \kappa = 0$). Let x be a coordinate along the normal $\boldsymbol{n}$ and y a coordinate along the binormal $\boldsymbol{b}$, according to figure 1. Then the position vector of any point in the duct may be written

$$\boldsymbol{r}(s,x,y) = \boldsymbol{r}_c(s) + x\boldsymbol{n}(s) + y\boldsymbol{b}(s). \tag{7}$$

The present choice of x- and y-coordinate axes are appropriate for non-rotated cross-sections. For rotated or 'inclined' cross-sections, the x- and y-axes should instead be inclined to $\boldsymbol{n}$ and $\boldsymbol{b}$, so that the boundary conditions become easy to apply. This matter is further explored in Bolinder (1996). The so-called natural base vectors of the coordinate system (s,x,y), which are tangents to the coordinate curves, are given by

$$\left.\begin{aligned} \boldsymbol{a}_s &= \frac{\partial\boldsymbol{r}}{\partial s} = (1-\kappa x)\,\boldsymbol{t} - \tau y\boldsymbol{n} + \tau x\boldsymbol{b}, \\ \boldsymbol{a}_x &= \frac{\partial\boldsymbol{r}}{\partial x} = \boldsymbol{n}, \quad \boldsymbol{a}_y = \frac{\partial\boldsymbol{r}}{\partial y} = \boldsymbol{b}. \end{aligned}\right\} \tag{8}$$

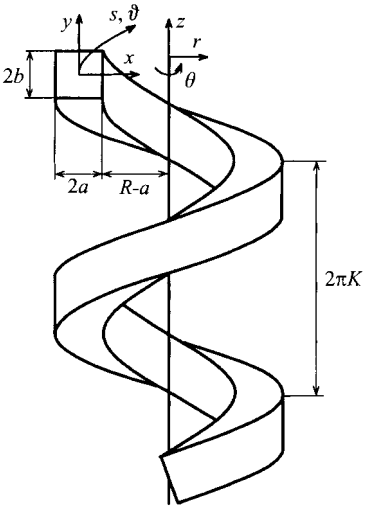

FIGURE 1. The helical square duct.

Thus, except for a toroidal duct (with $\tau = 0$), the natural base vectors are non-orthogonal for points off the centreline. By expanding the velocity vector in the natural basis, one obtains the contravariant velocity components v^s, v^x and v^y. Accordingly

$$\boldsymbol{v} = v^s \boldsymbol{a}_s + v^x \boldsymbol{a}_x + v^y \boldsymbol{a}_y. \tag{9}$$

However, if the natural basis is non-orthogonal, it is more convenient to expand the velocity in the physical basis $(\boldsymbol{t}, \boldsymbol{n}, \boldsymbol{b})$ according to

$$\boldsymbol{v} = w\boldsymbol{t} + u\boldsymbol{n} + v\boldsymbol{b}; \tag{10}$$

w is then the axial flow, and u and v constitute the secondary flow. Note that, since $(\boldsymbol{t}, \boldsymbol{n}, \boldsymbol{b})$ is a physical (i.e. an orthonormal) basis, the physical velocity components w, u and v are obtained as the projections of the velocity vector on the respective base vectors. The contravariant and the physical velocity components are related by

$$v^s = w/M, \quad v^x = u + \tau y w/M, \quad v^y = v - \tau x w/M, \tag{11}$$

where

$$M = 1 - \kappa x.$$

To obtain a comparison of the consequences of using either contravariant or physical velocity components, consider the simple case of laminar fully developed flow in a straight circular duct. If there is no swirl, the secondary flow components u and v are zero. Since for the straight centreline both κ and τ are zero, we obtain from (11) that the contravariant and the physical velocity components coincide. Now, if we provide the centreline with a finite torsion, i.e. we rotate the x- and y-coordinate axes as we proceed along the duct, the physical secondary flow components u and v are still zero. The base vectors $\boldsymbol{n}$ and $\boldsymbol{b}$ are rotating along the duct, but the secondary flow components remain unchanged. If instead the flow is described using the contravariant components, we note from (11) that v^x and v^y are non-zero if $\tau \neq 0$. Further, by increasing τ, v^x and v^y can obtain arbitrary large values. In view of these consequences, it seems advisable to describe the flow using physical velocity components.

Essentially two methods have been used in the past to derive the governing equations. The method employed for example by Germano (1982, 1989) utilizes the fact that an orthogonal coordinate system is obtained if the x- and y-coordinate axes

are rotated with respect to $\boldsymbol{n}$ and $\boldsymbol{b}$ in a prescribed manner along the duct. The orthogonality makes it easier to derive the governing equations, but then the coordinates must be transformed to undo the rotation. The other method to obtain the governing equations utilizes standard tensor analysis (e.g. Sokolnikoff 1964) to derive the equations in terms of contravariant velocity components. To obtain the physical velocity components, the transformation given by (11) must then be employed. Note that the above two methods yield the same final result. Thus, the method by Germano (1982, 1989) makes no simplifying assumptions as claimed by some authors, e.g. Xie (1990) and Chen & Jan (1992, 1993). Using basic vector and tensor analysis one may instead derive the governing equations directly in terms of the coordinates s, x and y and the physical velocity components w, u and v, see Bolinder (1996). The continuity equation and the Navier–Stokes equations, assuming an incompressible and fully developed flow, are obtained as follows:

$$\frac{\partial}{\partial x}(Mu+\tau y w)+\frac{\partial}{\partial y}(Mv-\tau x w)=0, \tag{12}$$

$$\begin{aligned}
&\frac{\partial w}{\partial t}+\left(u+\frac{\tau y}{M}w\right)\frac{\partial w}{\partial x}+\left(v-\frac{\tau x}{M}w\right)\frac{\partial w}{\partial y}-\frac{\kappa}{M}wu \\
&\quad=-\frac{1}{\rho M}\left(\frac{\partial p}{\partial s}+\tau y\frac{\partial p}{\partial x}-\tau x\frac{\partial p}{\partial y}\right)-v\left\{\frac{\partial}{\partial x}\frac{1}{M}\left(-M\frac{\partial w}{\partial x}+\tau y\frac{\partial u}{\partial x}-\tau x\frac{\partial u}{\partial y}+\kappa w-\tau v\right)\right. \\
&\quad\left.-\frac{\partial}{\partial y}\frac{1}{M}\left(M\frac{\partial w}{\partial y}-\tau y\frac{\partial v}{\partial x}+\tau x\frac{\partial v}{\partial y}-\tau u\right)\right\},
\end{aligned} \tag{13a}$$

$$\begin{aligned}
&\frac{\partial u}{\partial t}+\left(u+\frac{\tau y}{M}w\right)\frac{\partial u}{\partial x}+\left(v-\frac{\tau x}{M}w\right)\frac{\partial u}{\partial y}+\frac{1}{M}w(\kappa w-\tau v) \\
&\quad=-\frac{1}{\rho}\frac{\partial p}{\partial x}-\frac{\nu}{M}\left\{M\frac{\partial}{\partial y}\left(\frac{\partial v}{\partial x}-\frac{\partial u}{\partial y}\right)\right. \\
&\qquad+\left(-\tau y\frac{\partial}{\partial x}+\tau x\frac{\partial}{\partial y}\right)\frac{1}{M}\left(-M\frac{\partial w}{\partial x}+\tau y\frac{\partial u}{\partial x}-\tau x\frac{\partial u}{\partial y}+\kappa w-\tau v\right) \\
&\qquad\left.-\frac{\tau}{M}\left(M\frac{\partial w}{\partial y}-\tau y\frac{\partial v}{\partial x}+\tau x\frac{\partial v}{\partial y}-\tau u\right)\right\},
\end{aligned} \tag{13b}$$

$$\begin{aligned}
&\frac{\partial v}{\partial t}+\left(u+\frac{\tau y}{M}w\right)\frac{\partial v}{\partial x}+\left(v-\frac{\tau x}{M}w\right)\frac{\partial v}{\partial y}+\frac{\tau}{M}wu \\
&\quad=-\frac{1}{\rho}\frac{\partial p}{\partial y}-\frac{\nu}{M}\left\{-M\frac{\partial}{\partial x}\left(\frac{\partial v}{\partial x}-\frac{\partial u}{\partial y}\right)\right. \\
&\qquad+\left(\tau y\frac{\partial}{\partial x}-\tau x\frac{\partial}{\partial y}\right)\frac{1}{M}\left(M\frac{\partial w}{\partial y}-\tau y\frac{\partial v}{\partial x}+\tau x\frac{\partial v}{\partial y}-\tau u\right) \\
&\qquad\left.+\kappa\left(\frac{\partial v}{\partial x}-\frac{\partial u}{\partial y}\right)-\frac{\tau}{M}\left(-M\frac{\partial w}{\partial x}+\tau y\frac{\partial u}{\partial x}-\tau x\frac{\partial u}{\partial y}+\kappa w-\tau v\right)\right\}.
\end{aligned} \tag{13c}$$

These equations correspond to (20)–(24) in Tuttle (1990). The corresponding equations can also be found in a paper by Todd (1986). The assumption of a fully developed flow means that all s-derivatives are set to zero, except for the pressure derivative

$g = -\partial p/\partial s$, which is assumed constant. Note also that the body force is assumed conservative, so that it may be included in the pressure p; p is thus a generalized pressure. At the boundary, the usual no-slip condition is assumed.

A stream function $\psi = \psi(x, y)$, which automatically satisfies the continuity equation (12), may be defined according to

$$\frac{\partial \psi}{\partial y} = Mu + \tau y w, \quad -\frac{\partial \psi}{\partial x} = Mv - \tau x w; \tag{14}$$

$\psi(x, y) =$ constant defines a three-dimensional surface, and $\nabla\psi$ is normal to this surface. For a given s, $\psi(x, y) =$ constant defines a curve in the $(\boldsymbol{n}, \boldsymbol{b})$-plane, and $\nabla\psi$ is orthogonal to the tangent of this curve. One can show that

$$\nabla\psi \cdot (u\boldsymbol{n} + v\boldsymbol{b}) = \tau w(xu + yv),$$

which means that, unless $\tau = 0$, so that the above expression is zero, the curves $\psi =$ constant do not define streamlines for the secondary flow $(u\boldsymbol{n} + v\boldsymbol{b})$. However, one finds that

$$\nabla\psi \cdot \boldsymbol{v} = 0,$$

which proves that the velocity is tangent to the surfaces $\psi =$ constant. That is, these surfaces define streamtubes for the velocity field. Note that, if the contravariant components v^x and v^y are used for the secondary flow, it is found that the curves $\psi =$ constant do define streamlines for this 'secondary flow'. ψ may thus be employed to get a picture of the contravariant components v^x and v^y. According to the Navier–Stokes equations (13), the 'convective velocities' in the convection terms are precisely the contravariant components. This holds also for the scalar transport equations, such as the energy equation, see Bolinder & Sundén (1996). Thus, the contravariant velocity components are useful if one wishes to explain the convective transport of heat and momentum, for example. Obviously, the contravariant components include both the convective transport by the secondary flow components u and v and the convective transport by the axial flow w in the cross-plane due to the rotating cross-section for $\tau \neq 0$. The latter transport may be easier to understand by considering a fluid element travelling in the direction of the tangent $\boldsymbol{t}$ only, i.e. with the secondary flow components u and v zero. In a duct with non-zero torsion, due to the 'rotating' walls, the fluid element will then occupy different locations in the cross-section at different axial positions, and it will appear as if the fluid element had non-zero secondary flow components. This apparent secondary flow consists of the terms $\tau y w/M$ and $\tau x w/M$ in (11). Note that, farther away from the centre-line, i.e. for large x and y, the apparent secondary flow becomes more important. Several previous authors on helical duct flows provide contour plots of ψ, for example Wang (1981), who studied low-Reynolds-number flow in a helical circular duct and found that ψ shows a one-vortex structure for a relatively small torsion. If the secondary flow described by u and v had been plotted for the same flow case, two symmetric counter-rotating vortices would have been obtained, as for a toroidally curved duct with zero pitch. This reflects the second-order influence of torsion on the flow in a helical circular duct.

Next to be derived are the first-order equations in ϵ and η. Dimensionless quantities are defined according to

$$\left.\begin{aligned} &(S, X, Y) = (s, x, y)/d_h, \quad (U, V, W) = (u, v, w)\, d_h/\nu, \\ &\Psi = \psi/\nu, \quad P = p d_h^2/\rho\nu^2, \quad \epsilon = \kappa d_h, \quad \eta = \tau d_h, \\ &Re = \overline{w} d_h/\nu = \overline{W}, \quad De = Re\,\epsilon^{1/2}, \quad Gn = \eta Re, \end{aligned}\right\} \tag{15}$$

where an overbar indicates mean value, and where the hydraulic diameter for a rectangular cross-section with half-width a and half-height b (see figure 1) is given by

$$d_h = 4\frac{ab}{a+b}. \tag{16}$$

Assuming that the duct is loosely coiled and twisted, i.e. $\epsilon \ll 1$ and $\eta \ll 1$, and that the secondary flow is small compared to the axial flow, the dependent variables may be expanded in power series in ϵ and η as follows:

$$W = W_0 + \epsilon W_\epsilon + \eta W_\eta + \ldots, \quad U = \epsilon U_\epsilon + \eta U_\eta + \ldots, \quad V = \epsilon V_\epsilon + \eta V_\eta + \ldots, \tag{17a,b,c}$$

$$\Psi = \epsilon \Psi_\epsilon + \eta \Psi_\eta + \ldots, \quad P = -GS + \epsilon P_\epsilon + \eta P_\eta + \ldots, \tag{17d,e}$$

where the dots indicate terms of higher order in ϵ and η. The dimensionless axial pressure gradient $-G$ is assumed constant, and it is further assumed that P_ϵ and P_η do not depend on S. The method to expand in both the parameters ϵ and η was first suggested by Tuttle (1990). It has the advantage that by letting $\eta = 0$, the flow in a toroidal duct with zero pitch is obtained, and by letting $\epsilon = 0$, the flow in a straight twisted duct is obtained. From (17) we also note that, if higher-order terms in ϵ and η are neglected (i.e. ϵ^2, η^2, $\epsilon\eta$ etc.), the flow in a helical duct with finite pitch can be viewed as a superposition of the flow in a toroidal duct and a straight twisted duct. For example, since a straight twisted duct of circular cross-section does not differ from the straight untwisted duct, U_η and V_η are zero for a circular cross-section. Then, owing to the superposition principle, we may conclude that torsion has no first-order effect on the secondary flow in a helical circular duct with finite pitch. However, for ducts of non-circular cross-section, U_η and V_η are likely to be finite, which implies that torsion has a first-order effect.

By substituting the series (17) in the governing equations (12) and (13), and collecting terms independent of ϵ and η, the usual Poisson's equation for the unperturbed axial flow W_0 is obtained, namely

$$\nabla^2 W_0 = -G \tag{18}$$

where

$$\nabla^2 = \frac{\partial^2}{\partial X^2} + \frac{\partial^2}{\partial Y^2}$$

is the Laplacian operator. Setting $\eta = 0$ and collecting terms of order ϵ, yields the first-order equations for the flow in a toroidal duct, which after eliminating the pressure terms in (13b, c) read

$$\nabla^2 W_\epsilon = (U_\epsilon + 1)\frac{\partial W_0}{\partial X} + V_\epsilon \frac{\partial W_0}{\partial Y} - XG, \tag{19}$$

$$\nabla^4 \Psi_\epsilon = 2W_0 \frac{\partial W_0}{\partial Y}, \tag{20}$$

where the bi-Laplacian operator is given by

$$\nabla^4 = \frac{\partial^4}{\partial X^4} + 2\frac{\partial^4}{\partial X^2 \partial Y^2} + \frac{\partial^4}{\partial Y^4}.$$

According to (14), the stream function Ψ_ϵ satisfies

$$\frac{\partial \Psi_\epsilon}{\partial Y} = U_\epsilon, \quad -\frac{\partial \Psi_\epsilon}{\partial X} = V_\epsilon. \tag{21}$$

Similarly, setting $\epsilon = 0$ and collecting terms of order η, yields the first-order equations for the flow in a straight twisted duct, namely

$$\nabla^2 W_\eta = (U_\eta + YW_0)\frac{\partial W_0}{\partial X} + (V_\eta - XW_0)\frac{\partial W_0}{\partial Y}, \tag{22}$$

$$\nabla^4 \Psi_\eta = -4G, \tag{23}$$

where Ψ_η satisfies

$$\frac{\partial \Psi_\eta}{\partial Y} = U_\eta + YW_0, \quad -\frac{\partial \Psi_\eta}{\partial X} = V_\eta - XW_0. \tag{24}$$

Equations (20) and (23) for the stream functions, with the present no-slip boundary condition, are analogous to the equation for small deflections of a thin clamped plate, see for example Timoshenko & Woinowsky-Krieger (1959). From the theory of plates, it is also known that, for a rectangular boundary, it is not possible to obtain a closed-form analytical solution of (20) and (23), and it is often better to search for an approximate solution by a numerical method.

According to (18)–(21), W_ϵ is antisymmetric with respect to $X = 0$. This means that W_ϵ gives no net contribution to the mean axial flow, which in turn implies that there is no effect on the friction factor. We may also conclude that torsion has no first-order effect on the mean axial flow or the friction factor, since W_η is antisymmetric with respect to both $X = 0$ and $Y = 0$. W_0 is proportional to G, and from (17*a*) we then obtain, if only terms up to first order in ϵ and η are considered, that W_0 is proportional to the mean axial flow, since W_ϵ and W_η do not contribute to the mean, as concluded above. W_0 is therefore also proportional to the Reynolds number, based on mean axial flow, i.e.

$$W_0 \sim Re. \tag{25}$$

Then, from (19)–(24), the following estimates are obtained:

$$\left.\begin{aligned} &U_\epsilon, V_\epsilon \sim Re^2; \quad W_\epsilon \sim Re^3, Re; \\ &U_\eta, V_\eta \sim Re; \quad W_\eta \sim Re^2. \end{aligned}\right\} \tag{26}$$

The strength of the secondary flow in a toroidal duct is thus to the first order proportional to $\epsilon Re^2 = De^2$, and the secondary flow in a straight twisted duct is proportional to $\eta Re = Gn$. The secondary flow in a helical duct with finite pitch, which to the first order is obtained as a superposition of the secondary flow in a toroidal and a straight twisted duct, is then proportional to the sum of ϵRe^2 and ηRe. This implies that, for sufficiently small Re, the torsion-dependent term dominates, and for increasing Re, the curvature-dependent term eventually dominates. From (26), we also note that the first-order curvature-dependent perturbation to the axial flow ϵW_ϵ dominates the torsion-dependent perturbation ηW_η in both the limits of high and low Re.

An implication of the estimates in (26) is that the first-order coefficients U_ϵ, V_ϵ and W_ϵ rapidly become large as the Reynolds number increases, and for a relatively small Re the first-order curvature-dependent solution deteriorates and gives unrealistic results. The first-order coefficients U_η, V_η and W_η, on the other hand, show a much milder increase with increasing Re, which suggests that the first-order torsion-dependent solution is accurate for relatively high Reynolds numbers.

Note that the above estimates, in principle, are applicable to ducts of arbitrary cross-sections. Owing to the symmetry of particular cross-sections, however, some of the first-order coefficients are occasionally zero. For a circular cross-section, for example, U_η, V_η and W_η are all zero, and for an elliptical cross-section, according to Germano (1989), U_η and V_η are finite, but W_η is zero.

3. Numerical procedure

The governing equations, i.e. the continuity equation (12) and the Navier–Stokes equations (13*a–c*), are discretized and solved according to the finite-volume method with a staggered grid, see Patankar (1980). A steady, incompressible and fully developed flow is assumed. Central differencing is employed throughout. In fact, the hybrid difference scheme was implemented, which implies that upwind differencing is employed for the convection terms for a grid Péclet number greater than two. However, for a uniform 41×41 grid and for the flow rates considered in this study, it was verified that no upwind differencing emerged from the hybrid scheme. The velocity–pressure coupling was handled by the SIMPLEC algorithm of Van Doormaal & Raithby (1984). Their recommended accelerated TDMA-solver was also found effective. A θ-value of 1.9 was used for both the momentum and the pressure-correction equations. Under-relaxation factors of 0.6, 0.6 and 0.8 were used for the u, v and w momentum equations, respectively, and the pressure was under-relaxed by a factor of 0.9. The accelerated TDMA-solver was used together with an ADI-technique: one sweep in each direction for the momentum equations, and then ten sweeps for the pressure–correction equation, at each iteration. The input to the computations was a previously converged solution with a new value of the negative pressure gradient g. The Reynolds number was then calculated from the converged solution. Convergence was forced to the maximum capacity of the computer, using single-precision arithmetic. This normally required about 500 iterations, except close to the so-called limit points, which for the present 'transient' solution procedure are characterized by an infinitely slow rate of convergence. A limit point marks the upper or lower limit of a solution branch, see further Bolinder (1995*b*), where the limit points for helical square ducts are accurately determined using h^2-extrapolation. Grid refinement studies using 61×61 and 81×81 grids together with h^2-extrapolation, indicated that the solutions obtained on a 41×41 grid are accurate within 1 %, based on comparisons of the friction factor for the various grids.

The zeroth- and first-order equations (18)–(24) are solved according to a procedure similar to that for the full equations, but a non-staggered 41×41 grid is employed, and since the pressure terms have been eliminated no handling of the velocity–pressure coupling is needed. To provide the boundary conditions for the stream functions Ψ_ϵ and Ψ_η, i.e. zero partial derivatives with respect to both X and Y, the nodal values closest to the walls are forced to zero. When solving (20) and (23) for the stream functions Ψ_ϵ and Ψ_η, an under-relaxation factor of 0.6 proved necessary, and about 5000 iterations were required for full convergence. The remaining equations involving the (ordinary) Laplacian operator required only 50 iterations, with no under-relaxation, for a full convergence. The solutions of the first-order equations are estimated to be accurate within 1 %, like the solutions of the full equations.

4. Results and discussion

4.1. *Evaluation of first-order solution for ducts of square cross-section*

As concluded in §2, for a duct with non-zero torsion contours of the stream function Ψ do not represent the secondary flow as described by U and V. Therefore, vector plots are employed to present the secondary flow. Figure 2 shows the first-order terms of the secondary flow for a toroidal duct with zero pitch, i.e. U_ϵ and V_ϵ, and for a straight twisted duct, i.e. U_η and V_η. For a toroidal duct, two symmetric counter-rotating cells are obtained, and for a straight twisted duct the fluid appears to be pushed by the

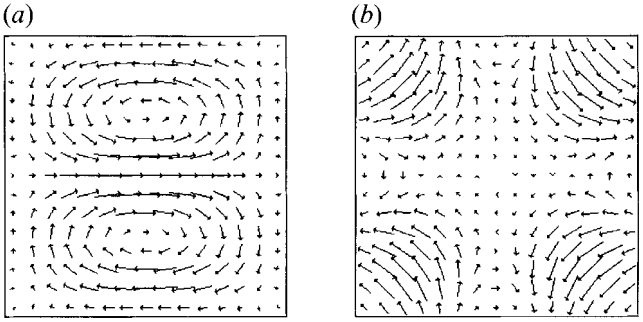

FIGURE 2. First-order solution of secondary flow in square ducts: (*a*) toroidal duct with outer wall to the right, (*b*) straight twisted duct.

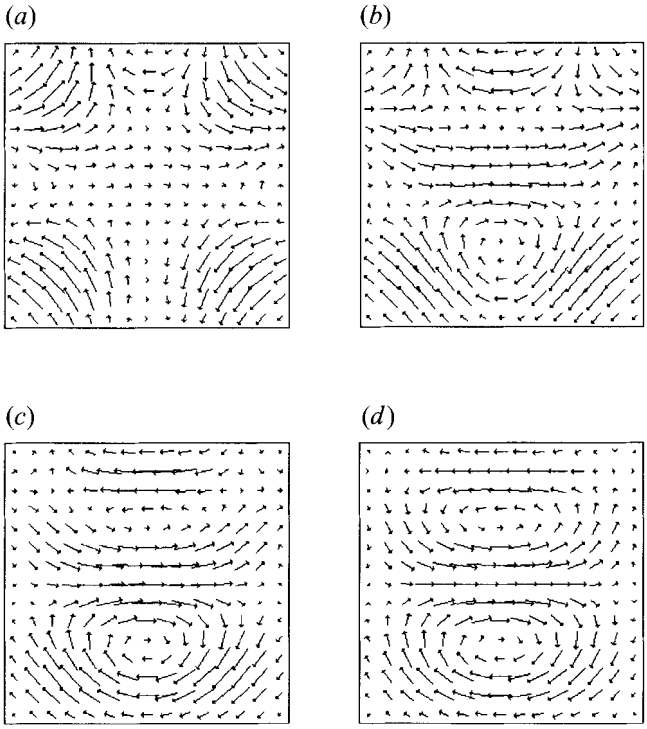

FIGURE 3. First-order solution of secondary flow in helical square ducts with $\epsilon = \eta$. Outer wall is to the right. (*a*) $Re = 2$, (*b*) $Re = 8.45$, (*c*) $Re = 20$, (*d*) $Re = 40$.

clockwise rotating walls, which gives a 'saddle flow' structure. Note that the appearance of the vector plots of the secondary flow to the first order are independent of the Reynolds number for both a toroidal and a straight twisted duct. However, as concluded previously, the strength of the secondary flow is proportional to $\epsilon Re^2 = De^2$ for a toroidal duct and to $\eta Re = Gn$ for a straight twisted duct. More specifically, according to a first-order analysis, the value of the maximum secondary flow in the cross-section relative to the Reynolds number, i.e. the mean axial flow, is given by

$$\frac{(U^2+V^2)^{1/2}_{max}}{Re} = \begin{cases} 0.017\epsilon Re \text{ for a toroidal square duct with zero pitch,} & (27a) \\ 0.144\eta \text{ for a straight twisted square duct.} & (27b) \end{cases}$$

The flow in a helical duct with finite pitch is to the first order obtained as a superposition of the flow in a toroidal and a straight twisted duct. Figure 3 shows the

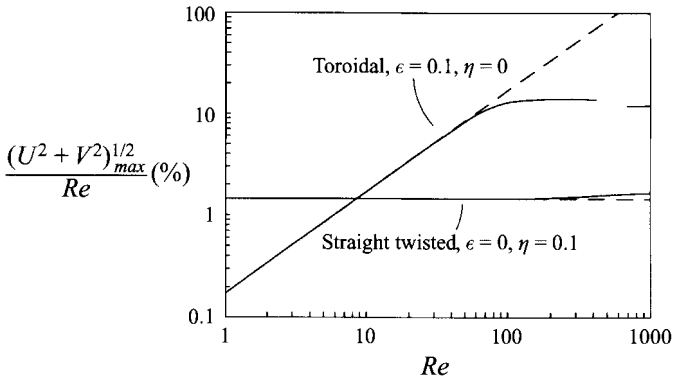

FIGURE 4. Maximum secondary flow in the cross-section relative to Re versus Re for toroidal and straight twisted square ducts. The solid line is from the numerical solution of the full equations and the dashed line is from the first-order solution.

first-order solution of the secondary flow in a helical square duct with $\epsilon = \eta$ for a few values of the Reynolds number. According to (6), a helical duct with $\epsilon = \eta$ (i.e. $\kappa = \tau$) has a pitch $2\pi K$ which is $2\pi \approx 6.3$ times the radius R, i.e. a fairly large pitch. From (27) it follows that the torsion-dependent contribution to the secondary flow dominates for small Re (figure 3*a*), and for increasing Re the curvature-dependent contribution eventually dominates (figure 3*d*). The respective contributions are of equal strength for $Re = 8.45$ (figure 3*b*).

Equations (27*a*, *b*), for $\epsilon = \eta = 0.1$, are plotted in figure 4 using dashed lines, together with data obtained from solutions of the full equations, using solid lines. For the toroidal duct, the first-order solution is relatively accurate up to a Reynolds number of about 60 ($De = 19$), where the overprediction is 6%. For higher Re, the first-order solution rapidly deteriorates. Actually, for Reynolds numbers greater than about 100 ($De > 32$), the relative strength of the secondary flow in the toroidal duct is approximately constant. Note that the gap in the solid line in figure 4 for Re between 415 and 681 is due to the finite extent of the S_1 and S_5 branches. The S_1 branch ends at $Re = 415$ ($De = 131$) and the S_5 branch begins at $Re = 681$ ($De = 215$), see further the discussion in the next subsection. For the straight twisted duct, according to figure 4 the first-order solution gives reasonable predictions for much higher Reynolds numbers. For example, for $Re = 500$ ($Gn = 50$), the relative strength of the secondary flow is underpredicted by 6% by the first-order solution.

Figure 5 provides some vector plots of the secondary flow obtained from the numerical solution of the full equations. For a toroidal duct with $\epsilon = 0.1$ and $Re = 60$ (figure 5*a*), the secondary flow is quite similar to the flow predicted by the first-order solution (figure 2*a*). The secondary flow vortices are shifted slightly towards the outer wall. If the curvature is increased to 0.4 (figure 5*b*), which implies that the Dean number is doubled from 19 to 38, the outward shift of the secondary flow vortices becomes more significant. For a straight twisted duct with $\eta = 0.1$ and $Re = 500$ ($Gn = 50$), according to figure 5(*c*) the secondary flow is very similar to the first-order prediction in figure 2(*b*). A dimensionless torsion η of 0.1 implies that the walls of the straight twisted duct rotate one complete turn over an axial distance of $2\pi/\eta \approx 63$ hydraulic diameters. For the case of $\eta = 0.4$ and $Re = 500$ ($Gn = 200$), shown in figure 5(*d*), the secondary flow vectors appear to be orientated along straighter paths between the walls, but the strength of the secondary flow is still only underpredicted by 6% by the first-order solution. According to the first-order results in (27), for helical ducts

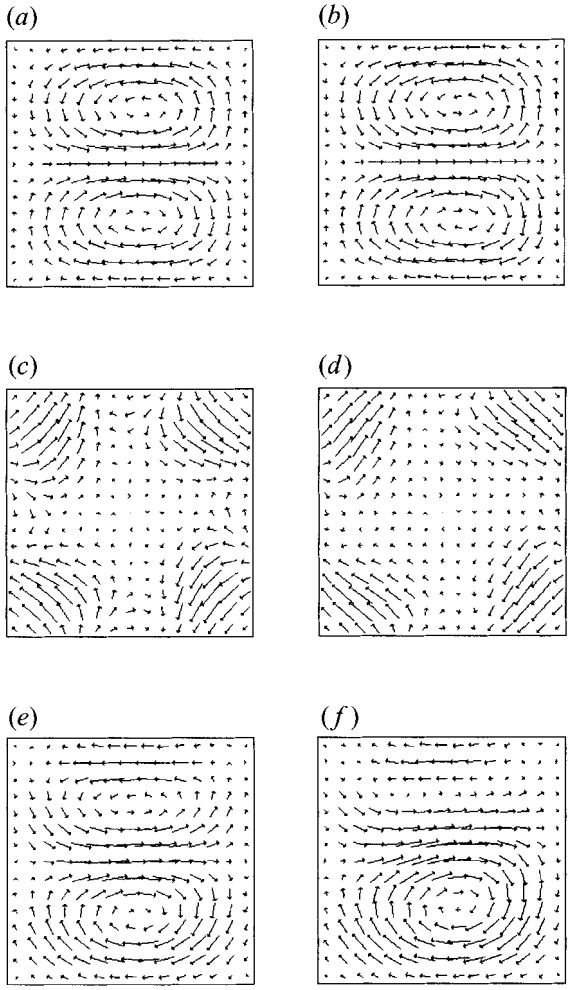

FIGURE 5. Vector plots of secondary flow obtained from the numerical solution of the full equations: (*a*) $\epsilon = 0.1$, $\eta = 0$, $Re = 60$; (*b*) $\epsilon = 0.4$, $\eta = 0$, $Re = 60$; (*c*) $\epsilon = 0$, $\eta = 0.1$, $Re = 500$; (*d*) $\epsilon = 0$, $\eta = 0.4$, $Re = 500$; (*e*) $\epsilon = \eta = 0.1$, $Re = 40$; (*f*) $\epsilon = \eta = 0.4$, $Re = 40$.

with the same ratio of curvature to torsion ϵ/η the appearance of the vector plots of the secondary flow depend only on the Reynolds number. For $\epsilon = \eta = 0.1$ and $Re = 40$, according to figure 5(*e*) the secondary flow is well predicted by the first-order solution in figure 3(*d*). For the higher value of $\epsilon = \eta = 0.4$ shown in figure 5(*f*), however, a significant enlargement of the lower secondary flow vortex, at the expense of the upper vortex, is observed, and the centre of the lower vortex is shifted towards the outer wall. In view of the above results for toroidal ducts with zero pitch, the shift towards the outer wall may be attributed to a higher-order effect of curvature alone. The enlargement of the lower vortex, however, cannot be attributed to a pure higher-order effect of torsion, which is very small at this low Re, but must be due to a combined higher-order effect of curvature and torsion (i.e. proportional to $\epsilon\eta$, $\epsilon^2\eta$ or $\epsilon\eta^2$, for example).

Vector plots of the contravariant components v^x and v^y are shown in figures 6(*a*) and 6(*b*) for the same cases as in figures 5(*d*) and 5(*f*) respectively. For a toroidal duct with zero pitch, v^x and v^y coincide with the secondary flow components u and v. For a

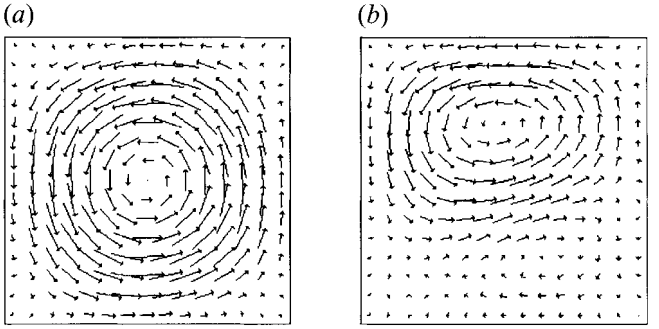

FIGURE 6. Vector plots of contravariant components v^x and v^y: (a) $\epsilon = 0$, $\eta = 0.4$, $Re = 500$; (b) $\epsilon = \eta = 0.4$, $Re = 40$.

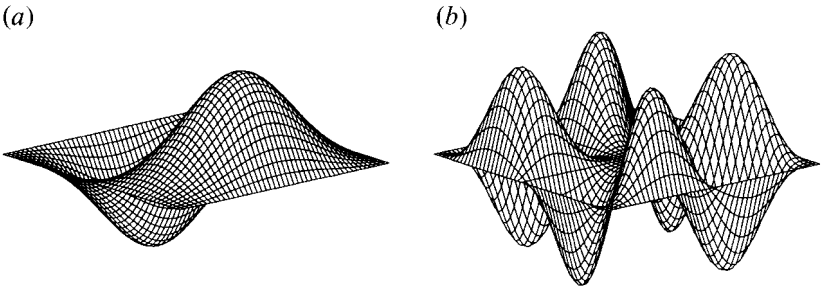

FIGURE 7. First-order perturbations of axial flow: (a) W_ϵ at $Re = 60$, viewed from outer wall; (b) W_η.

straight twisted duct (figure 6*a*), the contravariant components describe a counterclockwise swirl-like motion, quite different from the clockwise-oriented secondary flow in figure 5(*d*). For the helical duct in figure 6(*b*) the contravariant components describe a two-vortex structure with a dominating upper vortex, i.e. the opposite behaviour to the secondary flow in figure 5(*f*).

The first-order perturbations of the axial flow W_ϵ and W_η are shown in the three-dimensional plots in figure 7. The plot of W_ϵ in figure 7(*a*) is for a Reynolds number of 60. For this Re, the convection terms in (19) (those containing U_ϵ and V_ϵ) are dominating, and W_ϵ is essentially proportional to Re^3. W_ϵ is positive at the outer half of the cross-section and negative at the inner half. The net effect on the axial flow is accordingly a shift of the maximum towards the outer wall. For Reynolds numbers smaller than about 10, W_ϵ is instead proportional to Re, and contributes to a small shift of the axial flow towards the inner wall. The counteracting terms on the right-hand side of (19) balance each other at a Reynolds number of about 20, and for this Re no shift of the axial flow is obtained. The first-order perturbation of the axial flow due to torsion, i.e. W_η, is shown in figure 7(*b*). The form of W_η is the same for all Reynolds numbers, and the strength is proportional to Re^2. W_η contributes to a counterclockwise 'rotation' of the axial flow profile, see figure 8(*c*, *d*) below. For a square cross-section, however, the effect is weak. For $\eta = 0.1$ and $Re = 500$, for example, the maximum of the torsion-dependent contribution ηW_η is only 0.8% of Re.

Contours of the axial flow for the same cases as in figure 5(*b*, *d*, *f*) are shown in figure 8. On the left are the results from the first-order analysis, and on the right the results from the full equations. For the smaller value of curvature and torsion of 0.1 in figure 5(*a*, *c*, *e*), the effect on the axial flow is small, and it is also well predicted by the first-

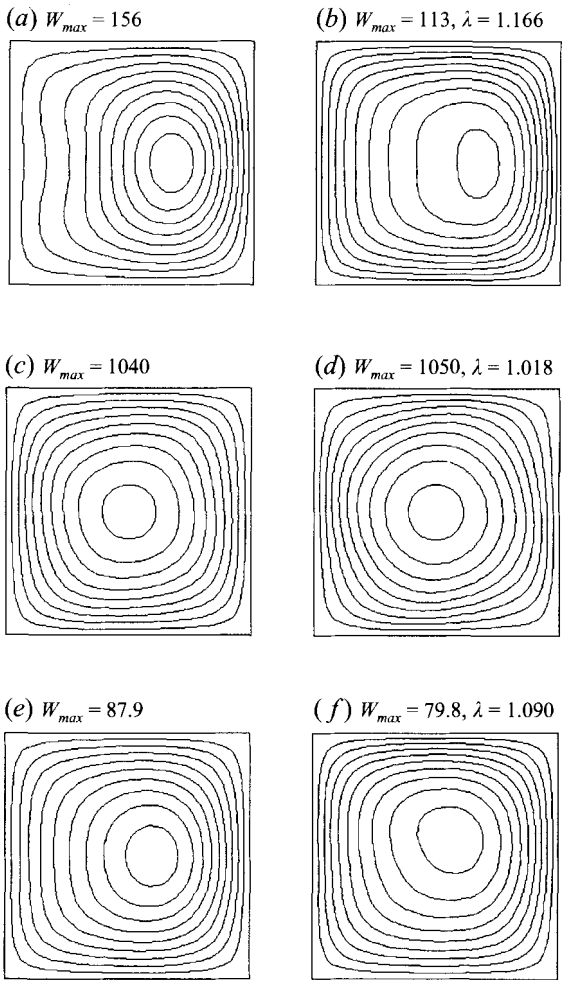

FIGURE 8. Contours of axial flow from the first-order solution (a, c, e) and from the solution of full equations (b, d, f). (a, b) $\epsilon = 0.4$, $\eta = 0$, $Re = 60$; (c, d) $\epsilon = 0$, $\eta = 0.4$, $Re = 500$; (e, f) $\epsilon = \eta = 0.4$, $Re = 40$.

order solutions. Figure 8(a, b) shows the axial flow for a toroidal duct at a Dean number of 38. The first-order solution overpredicts the maximum by 38%, and it underpredicts the wall gradients and consequently the friction factor. According to the solution of the full equations, the friction factor ratio $\lambda = fRe/(fRe)_s$ is 1.166 for the present case with $De = 38$, which is to be compared to the first-order prediction $\lambda = 1$. The index s in the expression for λ refers to a straight untwisted duct, for which $fRe = 14.22$ for a square cross-section. For the case in figure 5(a), with $De = 19$, λ is only 1.022. The deficiency of the first-order solution for $De = 38$ may be attributed to the relatively large error in the secondary flow as predicted by the first-order solution at this Dean number. The axial flow in a straight twisted duct with a Germano number of 200 is shown in figure 8(c, d). The maximum and the counterclockwise rotation of the contours are well predicted by the first-order solution. The solution of the full equations shows a slightly stronger rotation, and the central contours are more circular. The friction factor ratio λ is only 1.8% higher than the first-order prediction $\lambda = 1$. Finally, the axial flow in a helical duct with $\epsilon = \eta = 0.4$ and $Re = 40$ is shown

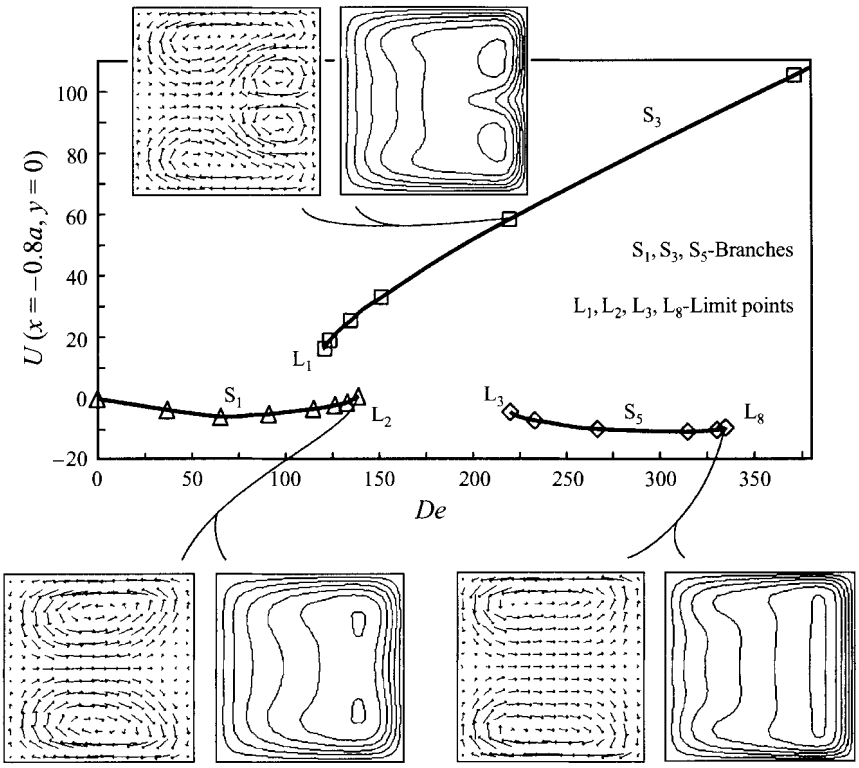

FIGURE 9. State diagram for toroidal square duct with $\epsilon = 0.2$. Secondary and axial flow at three states. Outer wall is to the right.

in figure 8(*e*,*f*). The maximum is overpredicted by 10% and the friction factor ratio is underpredicted by 8% by the first-order solution. The outward shift of the maximum is well captured by the first-order solution, but not the significant upward shift observed in the solution of the full equations. The upward shift of the maximum is due to the convective transport caused by the contravariant components depicted in figure 6(*b*). It must be due to a combined higher-order effect of curvature and torsion, since the upward shift is not observed for either a toroidal or a straight twisted duct. The effect can be qualitatively explained as follows: owing to torsion, the walls of the duct are rotating clockwise as one proceeds downstream; however the flow does not follow this rotation completely, but has a tendency to move straight forward in the duct; since the maximum axial flow is shifted outwards, owing to the effect of curvature, the 'incomplete' clockwise rotation of the flow is reflected as an upward shift of the maximum.

4.2. *Bifurcation structure for helical square ducts in the higher laminar regime*

For low enough Reynolds numbers, a unique and stable solution exists, which belongs to the so-called primary solution branch, labelled S_1 in the present study. For higher Reynolds numbers, additional solutions of branches other than the primary may appear. A limit point, or a one-sided bifurcation point, marks the upper or the lower limit of two connected solution branches, where at least one of the two branches is unstable, see further Benjamin (1978).

Figure 9 is a state diagram showing the detected solution branches for a toroidal square duct with $\epsilon = 0.2$. The vertical axis is the U-component of the secondary flow

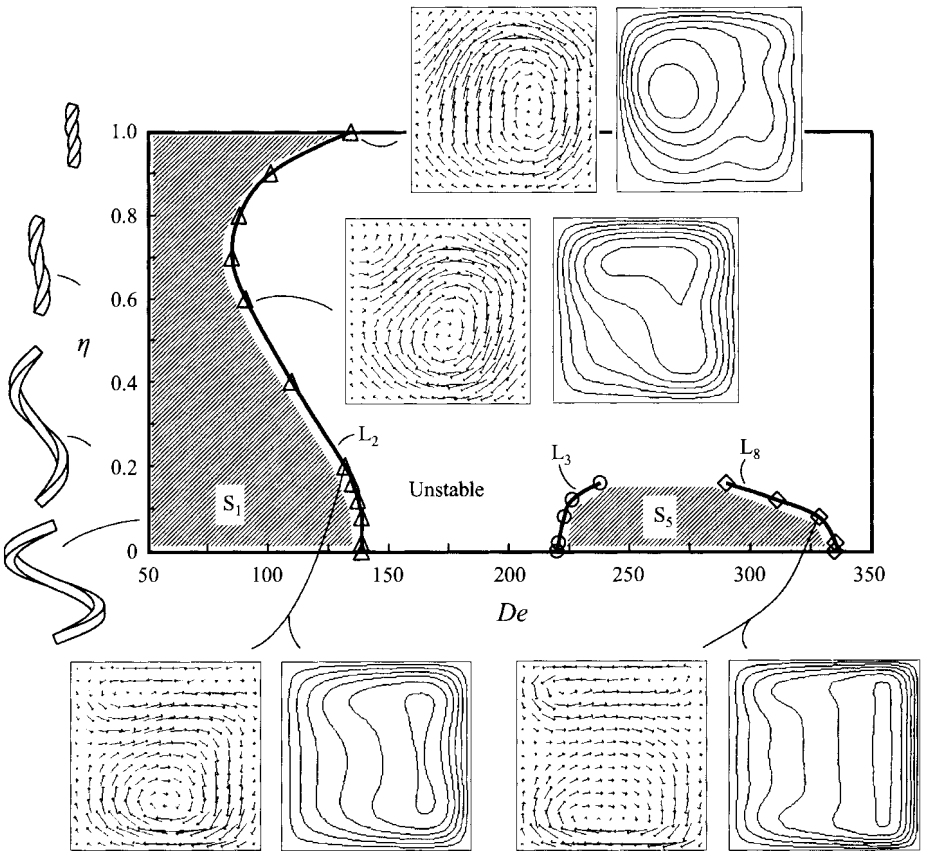

FIGURE 10. Extent of S_1 and S_5 branches for helical square ducts with $\epsilon = 0.2$. Secondary and axial flow at four states. Outer wall is to the right.

at a point close to the outer wall. Three branches were detected, denoted by S_1, S_3 and S_5, following Winters (1987). Note that since the present solution procedure is transient, only stable solution branches can be detected. Winters employed a 'direct' solution procedure, and he detected several unstable branches as well. The precise locations of the limit points were determined by Winters by solving an extended system of equations. In Bolinder (1995*b*), the limit points were instead found by utilizing the phenomenon that, for a transient solution method, the limit points are characterized by an infinitely slow rate of convergence. Using h^2-extrapolation, the results for the limit points by Bolinder (1995*b*) generally agreed well with the results by Winters (1987) and also Bara *et al.* (1992). According to figure 9, the primary S_1 branch ends at the limit point L_2 at a Dean number of 142. Note that the locations of the limit points, for ducts of finite curvature, depend to a slight extent explicitly on the curvature ϵ (apart from the implicit dependence via *De*). For a toroidally curved circular duct, S_1 extends to much higher Dean numbers. Yang & Keller (1986), for example, found for a toroidal circular duct an upper limit of S_1 at a Dean number of about 1600 (which approximately corresponds to their $D_1 = 25000$), but the result depended strongly on the number of terms retained in their series expansions, see also the related study by Yanase, Goto & Yamamoto (1989). For solutions of the S_1 branch near to L_2, according to figure 9, the secondary flow vortices are shifted towards the upper and lower walls, respectively, compared to the first-order solution in figure 2(*a*). This shift

is even more marked for solutions of the S_5 branch. S_5 is an unconditionally stable branch, with lower limit L_3 at $De = 230$ and upper limit L_8 at $De = 360$, for $\epsilon = 0.2$. Winters (1987) did not consider high enough Dean numbers to be able to determine L_8. Daskopoulos & Lenhoff (1989), however, report an upper limit of their corresponding branch, labelled 'e'. It was decided, after an examination of the bifurcation diagram of Daskopoulos & Lenhoff, to denote the upper limit of the S_5 branch by L_8. The S_3 branch is unstable to asymmetric perturbations, and could only be detected by imposing symmetry about the x-axis. Solutions of the S_3 branch have a pair of extra counter-rotating, so-called Dean vortices, at the outer wall. At the inflow region between these vortices, there is a deficit in the axial flow. The lower limit L_1 of S_3 is located at $De = 122$. No precise upper limit of S_3 was determined, but converged solutions were obtained up to a Dean number of about 550. The S_1 and S_3 branches are connected by a genuinely unstable branch, which is designated S_2 by Winters (1987). This branch could not be detected in the present study, however.

Figure 10 shows the extent of the S_1 and S_5 branches for helical square ducts with $\epsilon = 0.2$ and increasing torsion η; S_3 could not be detected for a finite torsion. Note that the pitch of the duct reaches a maximum where $\eta = \epsilon$, and that the duct with $\eta = 1$ closely resembles a straight twisted duct. For ducts of small torsion, both the flow field and the extent of the detected branches are similar to the conditions for a toroidal duct with the same dimensionless curvature ϵ. The lower vortex of the secondary flow is enlarged at the expense of the upper vortex, and the axial flow only shows a very slight asymmetry. For $\eta > 0.16$, the S_5 branch could not be detected, and the extent of the S_1 branch at first decreases, and for even higher torsion it then increases to higher Dean numbers again. For high enough torsion, the secondary flow approaches a one-vortex structure, and the maximum of the axial flow is shifted towards the inner wall. The shift of the maximum towards the inner wall for $\eta > 0.6$ can be explained by the fact that, for $\eta > 0.6$, a straight path opens up at the inner wall in the direction of the central axis, $r = 0$.

For completeness, the correlation for the friction factor ratio $\lambda = fRe/(fRe)_s$, reported in Bolinder (1995*b*), is repeated here:

$$\lambda = (1 + 0.288De + 8.8 \times 10^{-8} De^4)^{-0.3} + 0.107 De^{1/2}, \quad De < 1500, \quad \epsilon < 0.4, \quad \frac{\eta}{\epsilon} \leqslant 1. \tag{28}$$

Equation (28) gives correct values at the limits of both high and low Dean numbers, and for $\epsilon = 0.2$ it deviates by less than 2% from the computed values of the two-vortex branches. For $De < 6$, however, smaller error is obtained by using $\lambda = 1$. Equation (28) reflects the negligible influence of torsion on the friction factor ratio for $\eta \leqslant \epsilon$.

For certain Dean numbers, no unconditionally stable, fully developed flow solutions are obtained, as for example between the S_1 and S_5 branches, and above S_5. If one performs unsteady computations, for Dean numbers between L_2 and L_3, assuming fully developed conditions and no symmetry about the x-axis, the flow is found to oscillate regularly between a two-vortex and a four-vortex structure. For a helical square duct with a finite pitch, this is shown in Bolinder & Sundén (1995). An analogous behaviour is reported by Sankar *et al.* (1988) and Bara *et al.* (1992), in their steady and parabolic computations of developing flow in a toroidal square duct with zero pitch; for Dean numbers between L_2 and L_3, spatial oscillations develop, alternating between a two-vortex and a four-vortex structure. Mees (1994) continued the study of Bara *et al.* to higher Reynolds numbers. He also performed fully elliptic computations, assuming streamwise-periodic boundary conditions, and verified the

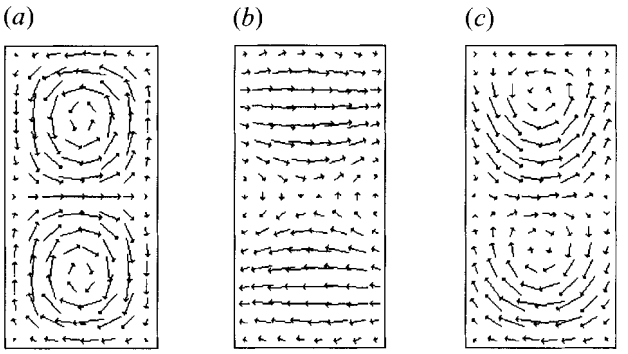

FIGURE 11. First-order solution of secondary flow in rectangular ducts with $b/a = 2$. Outer wall is to the right, where appropriate. (*a*) Toroidal duct, (*b*) straight twisted duct, (*c*) helical duct with $\epsilon = \eta$ and $Re = 80$.

existence of so-called 'twisting Dean vortices', a type of secondary instability phenomenon that previously has been observed in high-aspect-ratio curved channels, e.g. Matsson & Alfredsson (1990). In the experiments on helical duct flows with finite pitch by Bolinder & Sundén (1995), a steady two-vortex flow was normally obtained for Dean numbers between L_2 and L_3. Only by disturbing the flow at the duct inlet could a four-vortex flow occasionally be realized.

4.3. *Rectangular ducts of aspect ratio two*

Vector plots of the first-order solution of the secondary flow in rectangular ducts of aspect ratio $b/a = 2$ are shown in figure 11. For a toroidal duct with zero pitch, two symmetric counter-rotating cells are obtained. For a straight twisted duct, the fluid seems to be transported between opposite walls, in contrast to the twisted square duct, where the transport is between adjacent walls. The secondary flow in a helical duct with $\epsilon = \eta$ and $Re = 80$, which to the first order is obtained as a superposition of the flow in a toroidal and a straight twisted duct, is shown in figure 11(*c*). The effect of torsion is an upward shift of both of the secondary flow vortices.

The strength of the first-order contribution of the secondary flow relative to the mean axial flow, which for ducts of square cross-section is expressed by (27), for rectangular ducts of aspect ratio two is given by

$$\frac{(U^2+V^2)^{1/2}_{max}}{Re} = \begin{cases} 0.0092\epsilon Re \text{ for a toroidal duct with zero pitch,} & (29a) \\ 0.483\eta \text{ for a straight twisted duct.} & (29b) \end{cases}$$

Accordingly, the secondary flow strength in the toroidal rectangular duct is about half the strength obtained in a toroidal square duct, and the strength in the twisted rectangular duct is about three times the strength in a twisted square duct. These circumstances imply that torsion will have a more significant first-order impact on the secondary flow at higher Reynolds numbers in helical aspect-ratio-two ducts than in helical square ducts. In the vector plot in figure 11(*c*), for example, which is for $Re = 80$, the first-order effect of torsion is clearly visible, which would not have been the case for a duct of square cross-section at the same conditions. The curvature- and torsion-dependent contributions to the secondary flow are of equal strength when $(\epsilon/\eta)Re = 52.7$, compared to 8.45 for helical square ducts. The relation (29*a*) for a toroidal rectangular duct is accurate at higher Reynolds numbers than the corresponding relation (27*a*) for a toroidal square duct. For example, for $\epsilon = 0.1$ and

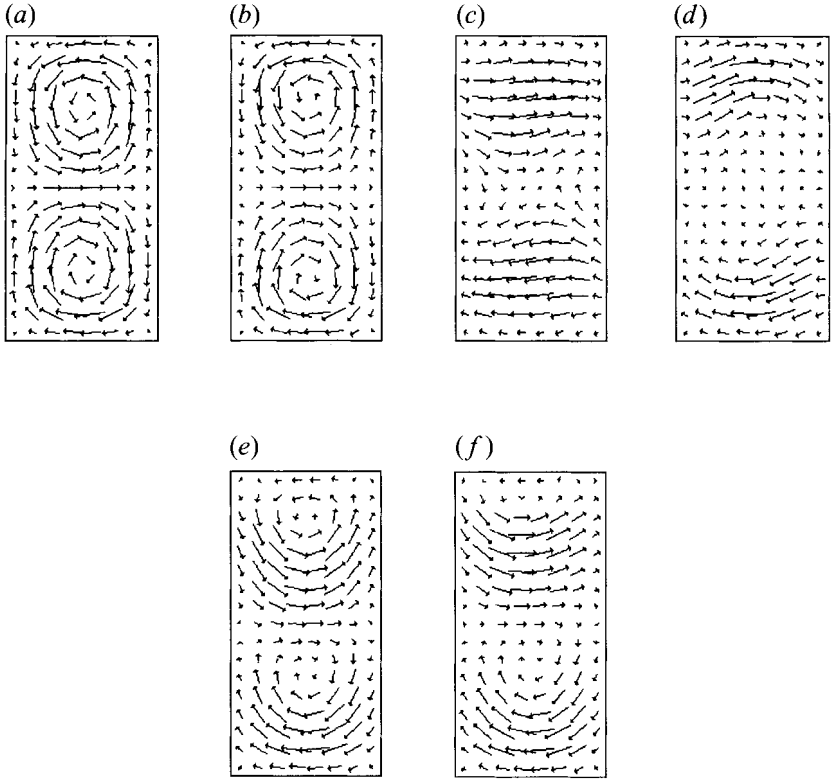

FIGURE 12. Vector plots of secondary flow obtained from the numerical solution of the full equations. (*a*) $\epsilon = 0.1$, $\eta = 0$, $Re = 80$; (*b*) $\epsilon = 0.4$, $\eta = 0$, $Re = 80$; (*c*) $\epsilon = 0$, $\eta = 0.1$, $Re = 320$; (*d*) $\epsilon = 0$, $\eta = 0.4$, $Re = 320$; (*e*) $\epsilon = \eta = 0.1$, $Re = 80$; (*f*) $\epsilon = \eta = 0.4$, $Re = 80$.

$Re = 80$ (i.e. $De = 25$), equation (29*a*) overpredicts the secondary flow strength by 4.5%. For a straight twisted duct, on the other hand, (29*b*) is less accurate at high Re than (27*b*); for $\eta = 0.1$ and $Re = 320$ (i.e. $Gn = 32$), (29*b*) underpredicts the secondary flow strength by 6%.

Vector plots of the secondary flow obtained from the numerical solution of the full equations are provided in figure 12. The plots in figure 12(*a*, *c*, *e*) for the lower values of ϵ and η, are all in good agreement with the first-order solutions in figure 11. Higher-order effects of curvature and torsion on the secondary flow are seen in figure 12(*b*, *d*, *f*), where ϵ and η are four times greater than in figure 12(*a*, *c*, *e*). For a toroidal duct with zero pitch, the secondary flow vortices shift towards the upper and lower walls, respectively. For a straight twisted duct, the secondary flow strength shows a relative decrease in the central part of the duct. For a helical duct finally, a (combined) higher-order effect of curvature and torsion is obviously an enlargement of the lower vortex of the secondary flow at the expense of the upper vortex, as was the case for a duct of square cross-section.

The contravariant components for the cases in figure 12(*d*, *f*) are shown in figure 13. As in the case of a square cross-section, the behaviour of the 'flow' described by v^x and v^y is quite different from the secondary flow.

The appearance of the first-order perturbation of the axial flow due to curvature, i.e. W_ϵ, is similar for a duct of aspect ratio two and for a square duct. For $Re < 25$, W_ϵ is positive at the inner half of the cross-section and negative at the outer half, and for $Re > 25$, the conditions are reversed. The first-order perturbation due to torsion, i.e. W_η,

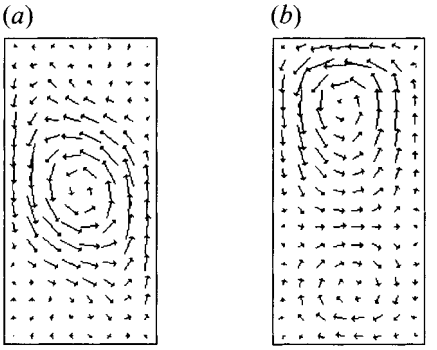

FIGURE 13. Vector plots of contravariant components v^x and v^y: (*a*) $\epsilon = 0$, $\eta = 0.4$, $Re = 320$; (*b*) $\epsilon = \eta = 0.4$, $Re = 80$.

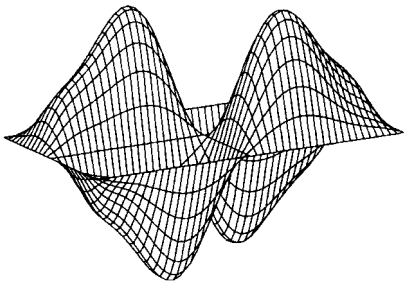

FIGURE 14. W_η for a rectangular duct with $b/a = 2$.

for a duct of aspect ratio two, differs more fundamentally from W_η for a square duct, as seen in figure 14. For a rectangular duct, W_η is no longer antisymmetric with respect to $x = y$ and $x = -y$. The maximum of W_η in the cross-section relative to Re equals $3.2 \times 10^{-4} Re$, which is twice the value obtained for a square duct.

Contours of the axial flow from the first-order solution and for the same cases as in figure 12(*b*, *d*, *f*) are shown in figure 15. In neither case is the first-order prediction accurate. For the straight twisted duct, the first-order solution predicts a slight clockwise rotation of the axial flow contours, while the rotation is actually counterclockwise and fairly strong. The specific form of the profile in figure 15(*d*) is explained by the convective transport caused by the contravariant components depicted in figure 13(*a*). Qualitatively, the form of the profile is explained by the clockwise-rotating walls, and the inability of the flow to follow the rotation completely. For the helical duct, a (combined) higher-order effect of curvature and torsion is as usual an upward shift of the maximum axial flow, which is caused by the convective transport by the contravariant velocity components shown in figure 13(*b*).

Regarding the bifurcation structure for higher Reynolds numbers, it was found by Shanthini & Nandakumar (1986) and Winters (1987) that the two-vortex branches S_1 and S_5 for a toroidal rectangular duct merge to one branch for an aspect ratio greater than 1.426. For an aspect ratio of two and $\epsilon = 0.2$, this is seen in the state diagram in figure 16. The upper limit L_2 of the primary S_1 branch is located at $De = 191$. The secondary flow vortices at L_2 are shifted markedly towards the upper and lower walls, respectively, and the axial flow contours are considerably elongated. A four-vortex branch, designated S_3, was also detected. The lower limit L_1 of S_3 was determined as $De = 108$, and an upper limit, designated L_3, was found at $De = 260$. As for a toroidal square duct, the S_3 branch is unstable to asymmetric perturbations.

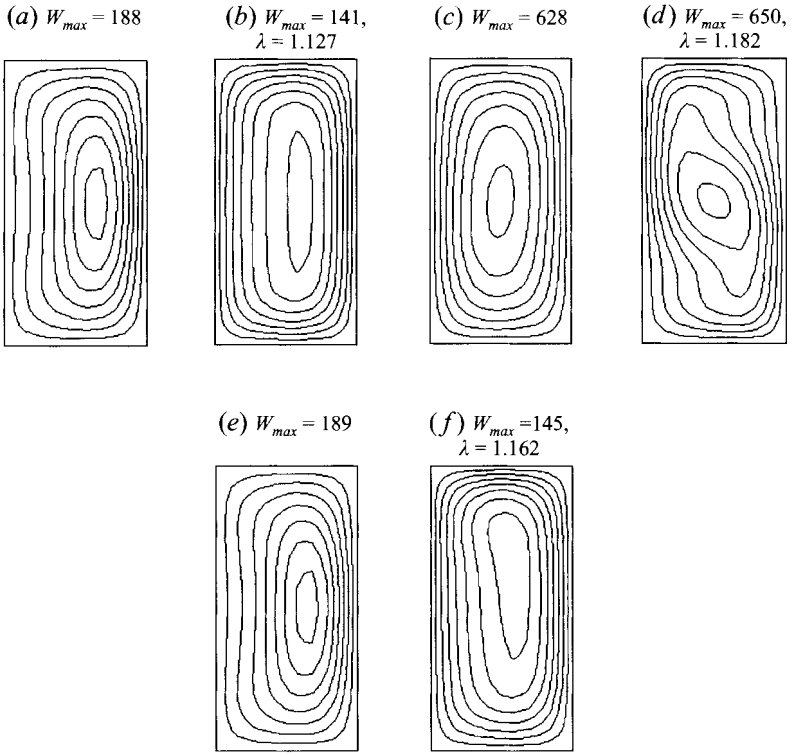

FIGURE 15. Contours of axial flow from the first-order solution (a, c, e) and from the solution of the full equations (b, d, f). (a, b) $\epsilon = 0.4$, $\eta = 0$, $Re = 80$; (c, d) $\epsilon = 0$, $\eta = 0.4$, $Re = 320$; (e, f) $\epsilon = \eta = 0.4$, $Re = 80$.

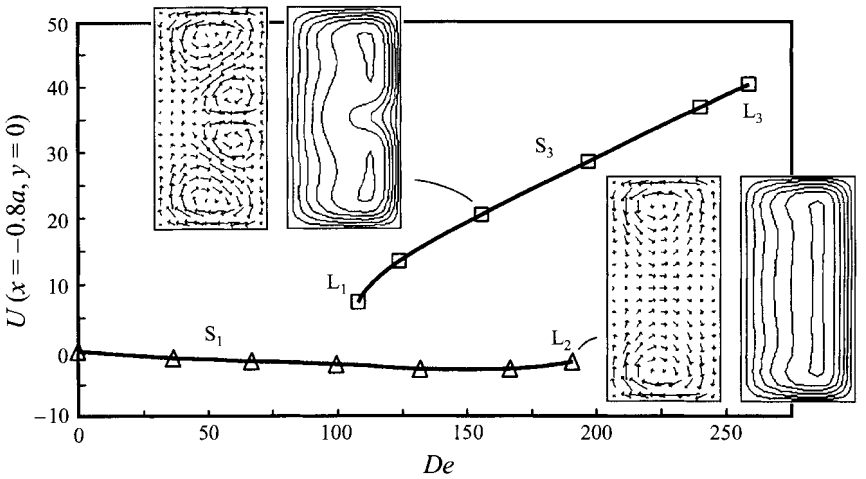

FIGURE 16. State diagram for a toroidal rectangular duct with $b/a = 2$ and $\epsilon = 0.2$. Secondary and axial flow at two states. Outer wall is to the right.

The extent of the S_1 branch for helical aspect-ratio-two ducts with $\epsilon = 0.2$ and varying torsion is shown in figure 17. The extent decreases more rapidly than for square ducts, and for $\eta > 0.9$ a slight increase is obtained. For $\eta = 0.2$ at L_2, the lower secondary flow vortex is considerably enlarged and the maximum axial flow is shifted towards the upper wall, and for $\eta = 1$ at L_2 the secondary flow describes a clockwise

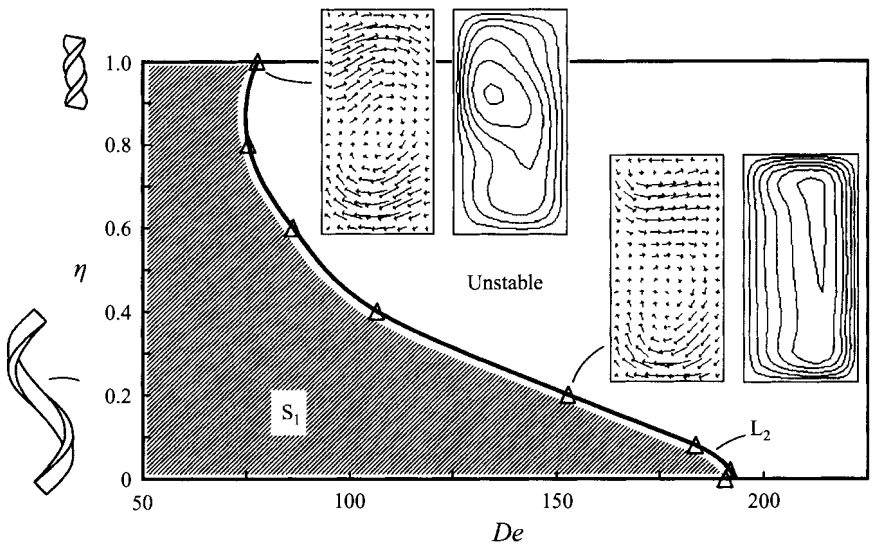

FIGURE 17. Extent of S_1 branch for helical rectangular ducts with $b/a = 2$ and $\epsilon = 0.2$. Secondary and axial flow at two states. Outer wall is to the right.

swirl-like motion, while the maximum axial flow is slightly shifted towards the inner wall.

5. Concluding remarks

The first-order contributions due to curvature ($W_\epsilon, U_\epsilon, V_\epsilon$) and due to torsion ($W_\eta, U_\eta, V_\eta$) of fully developed flow in square ducts and in rectangular ducts of aspect ratio two have been determined numerically. The secondary flow in a helical duct with a finite pitch or torsion is to the first-order obtained as a superposition of the secondary flow in a toroidal duct with zero pitch and a straight twisted duct. Thus, for a duct of circular cross-section, there is no first-order effect of torsion on the flow. For non-circular ducts, however, the secondary flow is dominated by torsion effects for sufficiently small *Re*, and for increasing *Re* the secondary flow is eventually dominated by effects due to curvature. For a square cross-section, the curvature- and torsion-dependent contributions to the secondary flow are of equal strength when $(\epsilon/\eta)\, Re = 8.45$, and for a rectangular cross-section of aspect ratio two when $(\epsilon/\eta)\, Re = 52.7$. Torsion has thus a stronger impact on the flow for an aspect ratio greater than one, which is not surprising.

The validity of the first-order solutions was determined from comparisons with solutions of the full governing equations. For a toroidal square duct with zero pitch, the first-order solution is fairly accurate up to a Dean number of about 20, where the friction factor ratio λ is underpredicted by 2% by the first-order solution. For a toroidal rectangular duct of aspect ratio two, the first-order solution has a similar accuracy up to $De = 25$. For a straight twisted square duct, the first-order solution is accurate at relatively high Germano numbers. At $Gn = 200$, for example, λ is only underpredicted by 2% by the first-order solution. This is to be compared to an underprediction of as much as 15% at $Gn = 128$ for a straight twisted duct of aspect ratio two. For ϵ and η up to 0.4, it was found that the explicit effects of ϵ and η are small, and that the flow is well correlated by *De* and *Gn* alone for toroidal and straight twisted ducts respectively.

For helical ducts of finite pitch, a significant higher-order effect of curvature and torsion was found to be an enlargement of the lower vortex of the secondary flow and a simultaneous shift of the maximum axial flow towards the upper wall. It was concluded that this effect is due to a combined effect of both curvature and torsion.

For higher Reynolds numbers, bifurcation phenomena appear. Three solution branches were detected for a toroidal square duct with zero pitch, and two branches were detected for a toroidal rectangular duct of aspect ratio two. For helical ducts of small pitch or torsion, the extent of the detected two-vortex branches is hardly affected by torsion, and for $\eta \leqslant \epsilon$, torsion has a negligible influence on the friction factor ratio λ.

To describe the flow, the physical velocity components w, u and v are employed. They are obtained from an expansion of the velocity vector in the physical basis $(\boldsymbol{t}, \boldsymbol{n}, \boldsymbol{b})$. The contravariant components v^x and v^y, which are obtained from an expansion of the velocity vector in the natural basis of the coordinate system, were found useful when describing the convective transport in the cross-plane of the duct. The contravariant components include both the convective transport by the secondary flow and the convective transport by the axial flow due to the rotating cross-section for $\tau \neq 0$.

The present series expansion analysis could, in principle, be continued by determination of the second-order and even higher-order terms in curvature and torsion. However, improvement of the first-order solution would most likely be obtained only for small Reynolds numbers. To obtain convergence of the series at higher Reynolds numbers, many terms need to be determined, and a method of extended Stokes series (Van Dyke 1978) would probably be needed. For ducts of rectangular cross-section, this is not a realistic task, in particular since no closed-form expressions for the terms can be obtained. For ducts of triangular cross-section, however, it would be possible to apply the method of extended Stokes series, as suggested by Nandakumar, Mees & Masliyah (1993), since the terms in a series expansion may be obtained in a closed form. Nandakumar *et al.* show that when the cross-section of the curved triangular duct is orientated such that the outer wall is flat, the state diagram is similar to the state diagram for a curved square duct.

REFERENCES

Bara, B., Nandakumar, K. & Masliyah, J. H. 1992 An experimental and numerical study of the Dean problem: flow development towards two-dimensional multiple solutions. *J. Fluid Mech.* **244**, 339–376.

Benjamin, T. B. 1978 Bifurcation phenomena in steady flows of a viscous fluid. *Proc. R. Soc. Lond.* A **359**, 1–43.

Berger, S. A. 1991 Flow and heat transfer in curved pipes and tubes. *AIAA Paper* 91-0030.

Berger, S. A., Talbot, L. & Yao, L.-S. 1983 Flow in curved pipes. *Ann. Rev. Fluid Mech.* **15**, 461–512.

Bolinder, C. J. 1993 Numerical visualization of the flow in a helical duct of rectangular cross-section. *Third Symp. on Experimental and Numerical Flow Visualization, New Orleans.* ASME FED-Vol. 172, pp. 329–338.

Bolinder, C. J. 1995*a* Observations and predictions of laminar flow and heat transfer in helical rectangular ducts. Doctoral thesis, Lund Institute of Technology, Sweden.

Bolinder, C. J. 1995*b* The effect of torsion on the bifurcation structure of laminar flow in a helical square duct. *Trans. ASME: J. Fluids Engng* **117**, 242–248.

Bolinder, C. J. 1996 Curvilinear coordinates and physical components – an application to the problem of viscous flow and heat transfer in smoothly curved ducts. *Trans. ASME: J. Appl. Mech.* (accepted).

BOLINDER, C. J. & SUNDÉN, B. 1995 Flow visualization and LDV measurements of laminar flow in a helical square duct with a finite pitch. *Exp. Thermal Fluid Sci.* **11**, 348–363.

BOLINDER, C. J. & SUNDÉN, B. 1996 Numerical prediction of laminar flow and forced convective heat transfer in a helical square duct with a finite pitch. *Intl J. Heat Mass Transfer* (accepted).

CHEN, W.-H. & JAN, R. 1992 The characteristics of laminar flow in a helical circular pipe. *J. Fluid Mech.* **244**, 241–256.

CHEN, W.-H. & JAN, R. 1993 The torsion effect on fully developed laminar flow in helical square ducts. *Trans. ASME: J. Fluids Engng* **115**, 292–301.

CHENG, K. C., LIN, R.-C. & OU, J.-W. 1976 Fully developed laminar flow in curved rectangular channels. *Trans. ASME: J. Fluids Engng* **98**, 41–48.

CUMING, H. G. 1952 The secondary flow in curved pipes. *Aeronaut. Res. Counc. RM* 2880.

DASKOPOULOS, P. & LENHOFF, A. M. 1989 Flow in curved ducts: bifurcation structure for stationary ducts. *J. Fluid Mech.* **203**, 125–148.

DEAN, W. R. 1927 Note on the motion of a fluid in a curved pipe. *Phil. Mag.* **4**, 208–223.

DEAN, W. R. 1928*a* The stream-line motion of fluid in a curved pipe. *Phil. Mag.* **5**, 673–695.

DEAN, W. R. 1928*b* Fluid motion in a curved channel. *Proc. R. Soc. Lond.* A **121**, 402–420.

DUH, T.-Y. & SHIH, Y.-D. 1989 Fully developed flow in curved channels of square cross sections inclined. *Trans. ASME: J. Fluids Engng* **111**, 172–177.

GERMANO, M. 1982 On the effect of torsion on a helical pipe flow. *J. Fluid Mech.* **125**, 1–8.

GERMANO, M. 1989 The Dean equations extended to a helical pipe flow. *J. Fluid Mech.* **203**, 289–305.

GHIA, K. N., GHIA, U. & SHIN, C. T. 1987 Study of fully developed incompressible flow in curved ducts, using a multi-grid technique. *Trans. ASME: J. Fluids Engng* **109**, 226–236.

ITO, H. 1951 Theory on laminar flows through curved pipes of elliptic and rectangular cross-sections. *Rep. Inst. High Speed Mech.*, vol. 1. Tohoku University, Sendai, Japan.

ITO, H. 1987 Flow in curved pipes. *JSME Intl J.* **30**, 543–552.

JOSEPH, B., SMITH, E. P. & ADLER, R. J. 1975 Numerical treatment of laminar flow in helically coiled tubes of square cross section. *AIChE J.* **21**, 965–974.

KAO, H. C. 1987 Torsion effect on fully developed flow in a helical pipe. *J. Fluid Mech.* **184**, 335–356.

KAO, H. C. 1992 Some aspects of bifurcation structure of laminar flow in curved ducts. *J. Fluid Mech.* **243**, 519–539.

KHESHGI, H. S. 1993 Laminar flow in twisted ducts. *Phys. Fluids* A **5**, 2669–2681.

LIU, S. & MASLIYAH, J. H. 1993 Axially invariant laminar flow in helical pipes with a finite pitch. *J. Fluid Mech.* **251**, 315–353.

LIU, S. & MASLIYAH, J. H. 1994 Developing convective heat transfer in helical pipes with finite pitch. *Intl J. Heat Fluid Flow* **15**, 66–74.

MASLIYAH, J. H. & NANDAKUMAR, K. 1981 Steady laminar flow through twisted pipes. *Trans. ASME: J. Heat Transfer* **103**, 785–796.

MATSSON, O. J. E. & ALFREDSSON, P. H. 1990 Curvature- and rotation-induced instabilities in channel flow. *J. Fluid Mech.* **210**, 537–563.

MEES, P. A. J. 1994 Instability and transitions of flow in a curved duct of square cross section. Doctoral thesis, University of Alberta, Canada.

MORI, Y., UCHIDA, Y. & UKON, T. 1971 Forced convective heat transfer in a curved channel with a square cross section. *Intl J. Heat Mass Transfer* **14**, 1787–1805.

MURATA, S., MIYAKE, Y., INABA, T. & OGAWA, H. 1981 Laminar flow in a helically coiled pipe. *Bull. JSME* **24**, 355–362.

NANDAKUMAR, K. & MASLIYAH, J. H. 1983 Steady laminar flow through twisted pipes: fluid flow and heat transfer in rectangular tubes. *Chem. Eng. Commun.* **21**, 151–173.

NANDAKUMAR, K. & MASLIYAH, J. H. 1986 Swirling flow and heat transfer in coiled and twisted pipes. In *Advances in Transport Processes*, vol. 4 (ed. A. S. Mujumdar & R. A. Mashelkar), pp. 49–112. Wiley.

NANDAKUMAR, K., MEES, P. A. J. & MASLIYAH, J. H. 1993 Multiple, two-dimensional solutions to the Dean problem in curved triangular ducts. *Phys. Fluids* A **5**, 1182–1187.

PATANKAR, S. V. 1980 *Numerical Heat Transfer and Fluid Flow*. McGraw-Hill.

SANKAR, S. R., NANDAKUMAR, K. & MASLIYAH, J. H. 1988 Oscillatory flows in coiled square ducts. *Phys. Fluids* **31**, 1348–1359.

SHANTHINI, W. & NANDAKUMAR, K. 1986 Bifurcation phenomena of generalized Newtonian fluids in curved rectangular ducts. *J. Non-Newtonian Fluid Mech.* **22**, 35–60.

SOH, W. Y. 1988 Developing fluid flow in a curved duct of square cross-section and its fully developed dual solutions. *J. Fluid Mech.* **188**, 337–361.

SOKOLNIKOFF, I. S. 1964 *Tensor Analysis.* Wiley.

THANGAM, S. & HUR, N. 1990 Laminar secondary flows in curved rectangular ducts. *J. Fluid Mech.* **217**, 421–440.

TIMOSHENKO, S. P. & WOINOWSKY-KRIEGER, S. 1959 *Theory of Plates and Shells.* McGraw-Hill.

TODD, L. 1986 Steady laminar flow through thin curved pipes. *Fluid Dyn. Res.* **1**, 237–255.

TUTTLE, E. R. 1990 Laminar flow in twisted pipes. *J. Fluid Mech.* **219**, 545–570.

VAN DOORMAAL, J. P. & RAITHBY, G. D. 1984 Enhancements of the SIMPLE method for predicting incompressible fluid flows. *Numer. Heat Transfer* **7**, 147–163.

VAN DYKE, M. 1978 Extended Stokes series: laminar flow through a loosely coiled pipe. *J. Fluid Mech.* **86**, 129–145.

WANG, C. Y. 1981 On the low-Reynolds-number flow in a helical pipe. *J. Fluid Mech.* **108**, 185–194.

WINTERS, K. H. 1987 A bifurcation study of laminar flow in a curved tube of rectangular cross-section. *J. Fluid Mech.* **180**, 343–369.

XIE, D. G. 1990 Torsion effect on secondary flow in a helical pipe. *Intl J. Heat Fluid Flow* **11**, 114–119.

YANASE, S., GOTO, N. & YAMAMOTO, K. 1989 Dual solutions of the flow through a curved tube. *Fluid Dyn. Res.* **5**, 191–201.

YANASE, S. & NISHIYAMA, K. 1988 On the bifurcation of laminar flows through a curved rectangular tube. *J. Phys. Soc. Japan* **57**, 3790–3795.

YANG, Z.-H. & KELLER, H. B. 1986 Multiple laminar flows through curved pipes. *Appl. Num. Math.* **2**, 257–271.